Published in final edited form as:
*Traffic*. 2010 July 1; 11(7): 972–986. doi:10.1111/j.1600-0854.2010.01066.x.

# Secretory Granule Membrane Protein Recycles Through Multivesicular Bodies

**Nils Bäck**[1], **Chitra Rajagopal**[2], **Richard E. Mains**[2], and **Betty A. Eipper**[2,3]

[1]Institute of Biomedicine/Anatomy, University of Helsinki, FIN-00014, Helsinki, Finland [2]Molecular, Microbial and Structural Biology, University of Connecticut Health Center, Farmington CT 06030-3401 [3]Neuroscience Department, University of Connecticut Health Center, Farmington CT 06030-3401

## Abstract

The recycling of secretory granule membrane proteins that reach the plasma membrane following exocytosis is poorly understood. As a model, peptidylglycine α-amidating monooxygenase (PAM), a granule membrane protein that catalyzes a final step in peptide processing was examined. Ultrastructural analysis of antibody internalized by PAM and surface biotinylation demonstrated efficient return of plasma membrane PAM to secretory granules. Electron microscopy revealed the rapid movement of PAM from early endosomes to the limiting membranes of multivesicular bodies and then into intralumenal vesicles. Wheat germ agglutinin and PAM antibody internalized simultaneously were largely segregated when they reached multivesicular bodies. Mutation of basally phosphorylated residues ($Thr^{946}$, $Ser^{949}$) in the cytoplasmic domain of PAM to Asp (TS/DD) substantially slowed its entry into intralumenal vesicles. Mutation of the same sites to Ala (TS/AA) facilitated the entry of internalized PAM into intralumenal vesicles and its subsequent return to secretory granules. Entry of PAM into intralumenal vesicles is also associated with a juxtamembrane endoproteolytic cleavage that releases a 100 kDa soluble PAM fragment that can be returned to secretory granules. Controlled entry into the intralumenal vesicles of multivesicular bodies plays a key role in the recycling of secretory granule membrane proteins.

### Keywords

secretory granule; endocytosis; multivesicular body; recycling; PAM; Intralumenal vesicles

## Introduction

Although local peptidergic secretory granule (SG) regeneration is not possible in neurons, endocrine or exocrine glandular cells, morphological and biochemical evidence indicates that many granule membrane proteins can be returned to SGs following exocytosis (1-10). It is also clear that exocytosis triggers the endoproteolytic cleavage of some granule membrane proteins, generating soluble cytoplasmic fragments targeted to the nucleus (11,12). The pathways through which granule membrane proteins generate cytoplasmic fragments or return to SGs following exocytosis are poorly defined. Retrograde endosomal transport to the trans-Golgi network (TGN) occurs from early endosomes and late endosomes/multivesicular bodies (13-15). Multivesicular bodies (MVBs) would be expected to play a key role in both processes,

Correspondence: Nils Bäck, Institute of Biomedicine/Anatomy, University of Helsinki, PB 63, 00014 University of Helsinki, +358-9-19125265 voice -19125261 fax, nils.back@helsinki.fi.

but their function has not been well characterized in cell types specialized in the storage and regulated secretion of peptides and proteins.

Using a neuroendocrine cell line, we studied the recycling of PAM, a SG membrane protein present in most neurons and peptide secreting endocrine cells (16). The trafficking of this type 1 integral membrane protein through the secretory and endocytic pathways is regulated by its 86 amino acid cytoplasmic domain (6,17). Phosphorylation at several sites in this domain was previously shown to control discrete steps in its endocytic trafficking (18,19) and its ability to generate a soluble, cytoplasmic fragment (12), but ultrastructural analyses were not carried out. Here we used both ultrastructural methods and surface biotinylation to study the fate of PAM traveling through the endocytic pathway. Using cell lines expressing PAM mutants, we show that the phosphorylation state of its cytoplasmic domain controls its entry into and exit from the intralumenal vesicles (ILV) of MVBs. PAM that enters into ILVs is more efficiently returned to the regulated secretory pathway than PAM that remains on the MVB limiting membrane.

## Results

### Plasma Membrane PAM Enters SGs

AtT-20 corticotrope tumor cells stably expressing PAM-1 at the level present in the anterior pituitary were studied; these cells store peptides derived from proopiomelanocortin (POMC) in SGs and release their content in response to secretagogue. PAM-1 is cleaved in SGs, generating soluble PHM (PHMs) and membrane PAL (PALm); the cleavage that generates soluble PAM (PAMs) plus TMD/CD does not occur in SGs (Fig. 1A). Based on both fluorescence and electron microscopy, PAM colocalizes with secretory products in the trans-Golgi network (TGN) area and in SGs at the tips of cellular processes (6,20-22;Fig. 1B). The steady state distribution of PAM overlaps and exceeds the distribution of TGN38, an established TGN marker (21;Fig. 1B), corresponding more closely to the distribution of syntaxin 6 (19;Fig. 1B), which has been localized to the TGN, immature SGs and endosomes (23-25). At steady state PAM shows limited colocalization with EEA1, an early endosomal marker, or cation independent mannose 6-phosphate receptor, a late endosomal marker (Fig. 1B). Electron microscopy localizes PAM to the TGN, MVBs and SGs; in late endosomes/MVBs, PAM accumulates in the membranes of ILVs (Fig.1C).

Less than 2% of the total PAM-1 is on the cell surface at steady state (26). Surface biotinylation coupled with subsequent secretagogue application was used to quantify the efficiency with which plasma membrane PAM-1 enters SGs (Fig. 1D). PAM-1 AtT-20 cells were exposed to cell impermeant activated biotin for 10 min at 37°C and the biotinylated PAM proteins released into the medium during subsequent chase incubations under basal and stimulated conditions were quantified using antibody to the linker region between PHM and PAL (Fig. 1A). For POMC, stimulated secretion is enriched in the cleavage products stored in SGs while basal secretion is enriched in intact POMC and partially cleaved intermediates (27). Biotinylated PAM-1 and PALm were detected in cells after a 10 min incubation with Sulfo-NHS-LC-biotin at 37°C (Fig. 1D, lower left). SGs contain large amounts of PHMs; the fact that PHMs was not biotinylated following incubation with biotin at 4°C for 1 h (not shown) or at 37°C for 10 min (Fig. 1D) demonstrates that biotinylation was limited to plasma membrane proteins.

PAM-1 biotinylated on the cell surface can remain intact, generate biotinylated cleavage products such as PHMs and PAMs or undergo degradation. During the 0-60 min chase, biotinylated PAMs and PHMs were released into the medium (Fig. 1D, lower right). The cleavage of PAM-1 that generates PHMs is catalyzed by prohormone convertases 1 or 2 and occurs in SGs. Cleavage close to the transmembrane domain yields PAMs, a product that is not readily detected in the biosynthetic pathway. Since these secreted biotinylated proteins

must be derived from biotinylated PAM-1, data were quantified as a percentage of biotinylated PAM-1 present at the end of the pulse (Fig. 1D, upper right). PALm can be biotinylated on the cell surface or created from biotinylated PAM-1, precluding its analysis. During the 0-60 min chase, about 4% of the biotinylated PAM-1 was released as PAMs or PHMs. After the 0-60 min chase, secretagogue treatment for 30 min stimulated the release of both biotinylated PAMs and PHMs two-fold over basal levels. Within 90 min of being on the plasma membrane, almost 10% of the biotinylated PAM-1 was converted into soluble proteins that were released over the next 90 min with secretagogue added.

## Stability of PAM-1 in the endocytic pathway

We used surface biotinylation to provide a quantitative assessment of the intracellular degradation of internalized PAM. PAM-1 biotinylated at the cell surface for 10 min at 37°C was analyzed immediately or allowed to traverse the endocytic pathway for 1 or 4 h before analysis (Fig.2A, B). Over half of the biotinylated PAM-1 present after the 10 min Pulse was recovered intact after a 1 h chase; over one-third remained intact after a 4 h chase (Fig.2C). As observed in the other biotinylation paradigm (Fig. 1D), about 4% of the biotinylated PAM-1 was converted into soluble products that were secreted during the first hour of chase (Fig. 2B,C). Secretion of PHMs occurred at a similar rate throughout the 4 h chase period. Although some of the PAM-1 biotinylated on the cell surface must be targeted to the lysosome for degradation, a significant fraction of it must be recycled.

## Internalized PAM/Ab complex enters early endosomes, MVBs and SGs

To identify the pathway through which plasma membrane PAM enters SGs, we utilized antibody uptake. To select appropriate times for analysis using electron microscopy, we compared the steady state localization of syntaxin 6 to the localization of internalized PAM/antibody complexes using immunofluorescence (Fig. 3A). Peripheral, round endosomes were labeled after 5 min of uptake and the first signs of trafficking to the peri-Golgi region were apparent by 10 min. After 20 min, PAM/antibody-containing endosomes were collected in the peri-Golgi region. The PAM-containing structures present after 40 and 60 min were smaller than those present at earlier time points. By 60 min, PAM/antibody complexes were concentrated in the TGN.

We next detected internalized PAM antibody with protein A-gold in cryosections at the ultrastructural level (Supplemental Table 1). Label was detected in tubular and vacuolar structures. The highest concentration was over MVBs. As shown earlier (21), most PAM-containing tubular or vacuolar structures were situated at some distance from the Golgi stack; the innermost TGN cistern showed no label. Labeling was low with this method and among the labeled vacuolar structures, immature SGs could not be reliably distinguished from endosomes; in cryosections, immature SGs lacked the electron dense core and electron lucent halo typically seen in conventional electron micrographs of these structures (28) (Supplemental Fig. 1).

At the light microscopic level, double staining for chromogranin A, a SG marker, showed accumulation of internalized PAM antibody in condensing granules in the TGN after 40 min of uptake (Fig. 3B). Double staining for ACTH in cryosections confirmed that internalized PAM-1 antibody was incorporated into SGs (Fig. 3C).

In order to obtain better morphological identification of the structures containing internalized PAM antibody, we utilized two additional techniques: We first detected the internalized antibody in fixed and permeabilized cells using anti-rabbit IgG coupled to 1.4 nm gold particles followed by silver intensification. With this method we could demonstrate the return of PAM/antibody complexes to the TGN and to nascent SGs with the typical morphology described

above (Fig. 3D,E). The localization of label corresponds to the distribution of internalized cationized ferritin, a general endosomal membrane marker (Fig. 3G). After 1 h of uptake, cationized ferritin was accumulated in MVBs and lysosomes. The TGN was also labeled, but only focally in peripheral tubules. In addition, label was seen in immature SGs (Fig. 3G). The silver intensification method is, however, not suitable for quantification, as the intensity of the signal and the background level vary between experiments.

We then used pre-formed PAM antibody/proteinA-gold complexes to follow the time course for internalization (Fig.4). After 1 min at 37°C, complexes were present in coated invaginations at the cell membrane. After 5 min, PAM/Ab/proteinA-gold complexes were at the peripheral membrane of round endosomes containing internal tubules. Following a 10 min chase, most of the complexes were on the outer membrane of rounded endosomes, which were extending tubules into their surroundings. PAM/Ab/proteinA-gold complexes were not observed in the extending tubules. After 20 min, PAM/Ab/proteinA-gold complexes appeared on the membranes of internal vesicles or tubules in round MVBs; the interior of these MVBs was uniformly electron dense. In some of these structures, gold particles were aggregated, and aggregated gold particles were also seen in lysosomes.

Following the 60 min chase, almost all of the gold particles had aggregated and were in lysosomes. The aggregated gold particles indicate that the internalized PAM/Ab/proteinA-gold complex was degraded, that the gold label had detached or that local conditions had atlered its appearance (29,30). With this method we could thus follow the entry of PAM into MVBs with high resolution, but could not detect its return to the TGN and to SGs.

## Incubation at 20°C arrests entry of PAM/Protein A-gold complexes into MVBs

Given the rapid uptake of PAM from the cell surface, we used low temperature as a means of distinguishing steps in the pathway. A 20°C temperature block allowed uptake of WGA-HRP, which binds to selected surface glycoproteins, or cationized ferritin into the interior of MVBs, but totally blocked their transport to the TGN (not shown). Based on fluorescence microscopy, internalized PAM/Ab complexes were arrested in peripheral, round endosomes and trafficking to the TGN was blocked (Fig. 5A). Electron microscopy identified these PAM-containing endosomes as MVBs (Fig. 5B,C). The 20°C temperature block slowed, but did not prevent entry of PAM/Ab/proteinA-gold complexes into the ILVs of MVBs. After the 60 min chase at 20°C, 60% of the PAM/Ab/protein A-gold complexes associated with MVBs remained on the limiting membrane (Fig. 5D). For comparison, when PAM/Ab/proteinA-gold complexes were internalized at 37°C, only 6% of the complexes remained on the limiting membrane after a 20 min chase (see Fig. 8B). Aggregation of gold complexes was not observed at 20°C. For both nonspecific membrane markers and for PAM, incubation at 20°C blocked trafficking to the TGN. The entry of PAM/Ab/proteinA-gold complexes into ILVs was more temperature sensitive than the entry of WGA-HRP or cationized ferritin. PAM/Ab/proteinA-gold complexes were not detected in cell organelles other than early endosomes and MVBs.

## Diversity in MVBs

To elucidate the dynamics of PAM uptake we studied simultaneous internalization of PAM antibody and WGA-Alexa Fluor 488 or WGA-HRP with live imaging and electron microscopy. Within 10 min, PAM/Ab was internalized into round endosomes mainly devoid of WGA. WGA uptake was tubular (31) and only a small minority of the PAM/Ab containing endosomes showed focal colocalization with WGA (Fig. 6A and Supplemental movie 1). More extensive colocalization of PAM/Ab and WGA was seen in endosomes in the TGN area (Fig. 6A). At the ultrastructural level, PAM/Ab was found in the periphery of round endosomes and WGA was found in tubules; some endosomal structures contained both (Fig. 6B,C). Further accumulation of PAM/Ab in the TGN area was mediated by a population of endosomes

undergoing fusion and fission events and conveying various amounts of WGA while exhibiting back and forth central and peripheral movements (Supplemental movie 1).

At the ultrastructural level, two types of endosomes were seen after 20 min of uptake (Fig. 6D,E). The first type (marked by arrowheads) were large WGA-containing vacuolar structures with ILVs at their margins and multiple WGA-containing tubules at their periphery; they had small amounts of PAM/Ab associated with the membranes of their vacuolar regions. The second type (marked by arrows) were MVBs that lacked WGA, extended few surrounding tubules and accumulated PAM/Ab in ILVs (Fig. 6D,E). The initial uptake of PAM/Ab is thus independent of the uptake of WGA. In late endosomes, PAM/Ab and WGA mixed, but the bulk of the PAM/Ab was routed to the interior of a subpopulation of MVBs devoid of WGA. Live imaging suggests that late endosomes make repeated contacts with early endosomes and the TGN.

A similar pattern of separation was seen when cells were first allowed to internalize PAM/Ab and WGA for 2 h at 20°C. No overlap of these markers was seen when internalization was arrested by the 20°C temperature block. Partial mixing was seen during further internalization at 37°C (Supplemental movie 2).

## Cytosolic domain phosphorylation regulates PAM trafficking through the internal vesicles of MVBs

Earlier studies identified $Thr^{946}$ and $Ser^{949}$ as substrates for casein kinase II and PCIP-2, a Ser/Thr protein kinase identified as a PAM Cytosolic Domain Interactor (32). PAM-1 phosphorylated at these sites is concentrated in the TGN region (Fig. 7A). Mutation of both sites to Ala, to prevent phosphorylation, or to Asp, to try to mimic phosphorylation, altered the endocytic trafficking of PAM (19). While PAM-1 and PAM-1/TS/AA have similar effects on the regulated secretory pathway and cytoskeletal organization, AtT-20 cells expressing PAM-1/TS/DD respond to secretagogue in much the same way as wildtype AtT-20 cells (19).

We utilized our PAM/Ab/protein A-gold uptake assay to compare the ability of these mutant PAM proteins to move through the endocytic pathway (Fig. 7B-D). Since our earlier studies localized differences in the trafficking of these mutant proteins to a step occurring after the 20° C block (19), we allowed cell lines expressing PAM-1, PAM-1/TS/AA or PAM-1/TS/DD to internalize and accumulate antibody for 1 h at 20°C. In all three lines, about 80% of the PAM/Ab/protein A-gold-containing structures were MVBs (Fig. 7B, C). A minor fraction of the gold particles were in round early endosomes lacking ILVs.

The temperature was raised to 37°C and endocytosis was allowed to continue for 15 min at 37°C. As for PAM-1, a significant fraction of the Ab/protein A-gold complexes internalized by PAM-1/TS/AA was converted into aggregates present in MVBs or lysosomes; for both PAM-1 and PAM-1/TS/AA, approximately one-third of the complexes remained unaggregated in MVBs. In contrast, in PAM-1/TS/DD cells, most of the gold-containing structures (84%) were still MVBs with membrane-associated, non-aggregated PAM/proteinA-gold complexes.

An even more dramatic difference was observed when the localization of the gold particles within MVBs was examined in detail (Fig. 7D). Data for cells exposed to 37°C for 15 min were quantified; gold particles associated with MVBs were categorized as associated with the limiting membrane or with ILVs. Ab/protein A-gold complexes internalized by PAM-1/TS/AA were almost entirely associated with the membranes of the ILVs; only 1% of the gold particles were associated with the MVB limiting membrane. In contrast, 39% of the Ab/protein A-gold complexes internalized by PAM-1/TS/DD were associated with the limiting membrane.

When the chase incubation was continued for 30 min at 37°C, the prevalence of aggregated gold particles increased. Fully 87% of the gold particles internalized by PAM-1 or PAM-1/TS/AA had aggregated by this time (Fig. 7B). When internalized by PAM-1, aggregates were prevalent in both MVBs and lysosomes. In contrast, when internalized by PAM-1/TS/AA, aggregates were much more likely to be associated with lysosomes. When internalized by PAM-1/TS/DD, only 58% of the gold particles had aggregated and aggregates were equally prevalent in MVBs and lysosomes.

## PAM cytosolic domain phosphorylation regulates MVB/lysosome traffic

To highlight differences between the mutant proteins, we incubated cells with PAM Ab/protein A-gold at 4°C followed by short chase incubations at 37°C (Fig. 8). After a 10 min chase, many of the Ab/protein A-gold complexes internalized by PAM-1 remained in early endosomes; very few aggregates were present, even though MVBs were heavily labeled (Fig. 8B). Complexes internalized by PAM-1/TS/AA moved more rapidly through the endocytic pathway. After a 10 min chase (Fig. 8B), 45% of the complexes internalized by PAM-1 TS/AA were associated with the membranes of ILVs; only 9-12% of the antibody internalized by PAM-1 or PAM-1 TS/DD had progressed to this point. After a 20 min chase (Fig. 8B), 48% of the complexes internalized by PAM-1/TS/DD were still localized to the outer membranes of the MVB. Most of the gold particles internalized by PAM-1 TS/AA had aggregated, while no aggregates were seen in PAM-1 TS/DD cells. These experiments suggest that phosphorylation of PAM at these sites prevents its entry into MVBs and that this step precedes aggregation of gold particles.

PAM-1/TS/AA enters the ILVs of the MVB more rapidly than PAM-1/TS/DD. To determine its ability to enter regulated SGs, we used the pre-embedding method (Fig. 9A). Antibody internalized by PAM-1-TS/AA cells was found in the Golgi area in round structures with an electron-dense core and an electron-lucent halo; this morphology is typical of immature SGs in AtT-20 cells (28). The identification of these structures as SGs was confirmed by colocalization of internalized antibody with ACTH (Fig. 9B) and the granule marker chromogranin A (Fig. 9C). Although PAM antibody internalized by PAM-1-TS/DD cells also accumulated in the trans-Golgi area, few of the structures that contained internalized antibody were positive for chromogranin A (Fig. 9D).

## Cytosolic domain phosphorylation regulates access of plasma membrane PAM to SGs

Modification of $Thr^{945}/Ser^{949}$ in the cytosolic domain of PAM alters PAM trafficking through MVBs and entry into granules. We turned to our biotinylation protocols to quantify the effect of these mutations on stability and access to SGs. When compared to PAM-1, plasma membrane levels of both PAM-1/TS/AA and PAM-1/TS/DD were increased about three-fold (PAM-1/TS/AA, 4.76±0.59% of total; PAM-1/TS/DD, 4.02±0.11% of total). PAM-1/TS/AA is expressed at lower levels than PAM-1, eliminating expression level as the cause of the increase in surface PAM. The pulse/chase protocol used to evaluate the stability of PAM-1 (Fig. 2) was used to assess PAM-1/TS/AA and PAM-1/TS/DD (Fig. 10A). As for PAM-1, approximately half of the PAM-1/TS/DD biotinylated during a 10 min labeling period at 37°C was recovered from cells or medium after 1 h of chase. PAM-1/TS/AA was more stable; about 80% of the biotinylated PAM-1/TS/AA could be accounted for after a 1 h chase (Fig. 10B); over 60% was recovered after a 4 h chase (data not shown). While the chase medium of PAM-1/TS/AA cells contained biotinylated PAMs, PAM-1/TS/DD cells secreted only PHMs (Fig. 10B).

To assess the effect of these mutations on the ability of plasma membrane PAM to enter SGs, the stimulated secretion paradigm was employed (Fig. 10C). During the 0-60 min chase, PAMs was the major biotinylated product released by PAM-1/TS/AA cells while PHMs was the major biotinylated product released by PAM-1/TS/DD cells. Basal secretion of PAMs from PAM-1/

TS/AA cells remained high during the 60-90 min chase period (Fig. 10D). Application of secretagogue during the 60-90 min chase stimulated release of both biotinylated PAMs and PHMs from PAM-1/TS/AA cells; over 16% of the biotinylated PAM-1/TS/AA present after the pulse labelling period was released in response to secretagogue. Biotinylated PAM-1/TS/DD yielded very little PAMs and application of secretagogue stimulated the release of only about 5% of the biotinylated PAM-1/TS/DD.

## Discussion

### Internalized PAM has access to SGs

Our knowledge about the recycling of SG membrane is largely based on early electron microscopic studies showing that internalized membrane markers are incorporated into newly formed SGs (1-4). Plasma membrane glycoprotein III (5), PAM (6), dopamine-β-hydroxylase (7), ICA512 (8), phogrin (9) and P-selectin, when expressed in neuroendocrine cells (10), each return to SGs. Sorting signals localized to the cytoplasmic tails of PAM (6,17), phogrin (9) and P-selectin (33) are essential to this process, although the routes taken have not been delineated.

PAM, which catalyzes one of the final steps in neuropeptide synthesis, is internalized from the plasma membrane, appears briefly in early endosomes and then enters MVBs. Concomitant with movement from the MVB limiting membrane into ILVs, PAM begins to accumulate in a perinuclear syntaxin 6 positive compartment. Syntaxin 6 is present in the TGN, but also in immature secretory granules, where it is needed for their fusion and maturation (see Ref 23), and in endosomes, where it is needed for retrograde transport to the TGN (24,25). Less than half of the PAM entering the endocytic pathway is degraded during the first hour and some is converted into PHMs, an active end product formed only in SGs. Lumenal cleavage near the transmembrane domain of internalized PAM generates PAMs, a product not formed in SGs (34). Taken together, our results indicate that MVBs are key sorting stations targeting internalized PAM to SGs or lysosomes. One factor known to affect sorting in MVBs is the availability of copper (35), an essential component of the active site of PAM; return to granules is favored when copper levels are low.

### How you look affects what you see

Antibody/proteinA-gold complexes provided high resolution images of the early events in PAM endocytic trafficking. However, the appearance of gold aggregates suggested dissociation of antigen/antibody complexes, making it impossible to track the protein of interest. In addition, bulky lumenal labels can affect protein routing (36). To overcome these limitations, we used several approaches. Staining of cryosections identified PAM in the interior of MVBs at steady state (Fig. 1C). We tracked uptake of PAM antibody not labeled with gold into the interior of MVBs (Supplemental Table 1 and Fig. 3D,F). Surface biotinylation was used to quantify stability and return to granules since this small label is less likely to affect trafficking or to be removed.

Although aggregated gold particles do not mark the location of internalized PAM, the fact that aggregates form differently when antibody/gold complexes are internalized by PAM-1/TS/AA or PAM-1/TS/DD indicates differences in routing. Unbound or protein bound protein A-gold does not aggregate in conditions used for cryostaining. Aggregation can be induced by low pH or high electrolyte concentration (37), conditions that could occur in MVBs (29,30). As seen with BSA-gold in lysosomes (38), aggregation could be induced by proteolytic degradation in the acidifying MVB; however, the stability of PAM-TS/AA, which enters MVBs more effectively than PAM-TS/DD, argues against this.

### Intralumenal vesicles have many roles

In yeast, ubiquitinated proteins destined for vacuolar degradation are collected and invaginated into ILVs by the ESCRT complex (39,40). Mammalian MVBs are more complex, with additional mechanisms of entry (41-43), different types of MVB and different types of ILV (44,45). Proteins that enter mammalian ILVs can be secreted as exosomes (46), undergo backfusion with the limiting membrane of the MVB (30,47-49) or travel to lysosomes. In neurons, temporal and spatial regulation of signaling is controlled by sheltering signaling receptors inside MVBs (50-52) and MVBs mediate transcytosis of adhesion molecules from dendrites to axons (53). Tetraspanins and cholesterol, which are enriched in ILVs, escape routing to lysosomes (54-56).

We show that entry of internalized PAM into ILVs is not necessarily associated with degradation. PAM-1/TS/AA, which enters ILVs more efficiently than PAM-1/TS/DD, is degraded less extensively than PAM-1/TS/DD. PAM joins a short list of proteins including tetraspanins, MHC class II complexes, anthrax toxin and vesicular stomatitis virus (57) that are incorporated into ILVs and escape lysosomal degradation. The exit of PAM from ILVs is not linked to cholesterol; neither cholesterol depletion by lovastatin treatment nor treatment with U18666A, which makes cholesterol accumulate in late endosomes, affected PAM trafficking (Bäck, unpublished). In contrast, U18666A treatment arrested internalized CI-MPR in MVBs in both HeLa (58) and AtT-20 cells; when arrested in AtT-20 cell MVBs, CI-MPR entered ILVs (Bäck, unpublished).

### Phosphorylation regulates PAM entry into ILVs

The unstructured cytoplasmic domain of PAM is multiply phosphorylated; many sites, including $Ser^{949}$, are phosphorylated under basal conditions (12). $Ser^{949}$ can be phosphorylated by casein kinase II and by P-CIP2/KIS/UHMK1, a kinase that binds PAM at a site distinct from its phosphorylation site (22,32). The ability of PAM to interact with P-CIP2 is essential to the ability of PAM to alter cytoskeletal organization and inhibit regulated secretion (22). Mutation of the casein kinase II/P-CIP2 sites to Asp yields PAM-1/TS/DD, an active enzyme that is unable to alter cytoskeletal organization or inhibit regulated secretion. PAM-1 mutated to Ala at these same sites alters cytoskeletal organization and regulated secretion in the same way as native PAM-1.

Mutation of $Ser^{949}$ and $Thr^{946}$ was without effect on the movement of PAM through the early endocytic pathway, but both phosphorylation and dephosphorylation at these sites play essential roles later in the endocytic pathway. PAM-1/TS/AA enters ILVs rapidly while PAM-1/TS/DD remains on the MVB limiting membrane, suggesting that dephosphorylation of this site regulates ILV entry. The fact that surface biotinylated PAM-1/TS/AA is more stable than surface biotinylated PAM-1/TS/DD suggests that ILV entry is not directly associated with turnover. Based on the amount of surface biotinylated protein subsequently released in response to secretagogue, internalized PAM-1/TS/AA enters SGs more efficiently than internalized PAM-1/TS/DD (Fig. 10D). The trigger for dephosphorylation of PAM could be a conformational change transmitted to the cytosolic domain following acidification of the luminal domain inside the MVB (59).

### PAM undergoes a sheddase-type cleavage in the MVB

PAM-1 that is biotinylated on the cell surface is cleaved near its transmembrane domain to produce PAMs. Metabolic labeling experiments indicate that PAMs is not produced in the biosynthetic pathway (20). While biotinylated PAMs is released from PAM-1 AtT-20 cells under basal and stimulated conditions, it is a minor product; biotinylated PHMs, the product of a SG cleavage, is the major product. In contrast, PAMs is the major product released from PAM-1/TS/AA cells. Almost no biotinylated PAMs is released from PAM-1/TS/DD cells.

Ectodomain cleavages of this type are often accomplished by sheddases or secretases of the metalloprotease or ADAM families (60,61). Best known are the secretases which cleave amyloid precursor protein. Amyloid precursor protein is also cleaved within the endosomal system, yielding soluble products that are secreted (62-65). Elimination of CI-MPR involves sheddase-type cleavage followed by luminal domain secretion (66,67) rather than lysosomal degradation (68).

The different cleavage patterns observed for biotinylated PAM-1/TS/AA and biotinylated PAM-1/TS/DD may reflect differences in their localization or in their structure. If differences in localization are critical, these are first apparent in MVBs, with PAM-1/TS/DD remaining on the limiting membrane of the MVB while PAM-1/TS/AA enters the ILVs. Taken together, our data suggest that occurrence of the sheddase-type cleavage is associated with ILV entry; cleavage could be essential for ILV entry or could occur in ILVs. Wherever it is generated, PAMs has access to a secretagogue-responsive compartment, since its release is stimulated when phorbol ester and $BaCl_2$ are added to the culture medium. The sheddase-type cleavage that generates PAMs also generates a transmembrane domain/cytoplasmic domain fragment of PAM-1 (Fig. 1A). Cleavage of PAM-1 within its transmembrane domain was recently shown to yield a soluble cytoplasmic fragment of PAM (sf-CD) that localizes to the nucleus (12). PAM-1/TS/DD yields very little sf-CD. Since intramembrane proteolysis of this type generally requires removal of the luminal domain, it is tempting to suggest that production of sf-CD is also associated with entry into ILVs.

## Materials and Methods

### Cells

AtT-20 mouse pituitary corticotropic tumor cell lines stably expressing PAM-1 (20), PAM-1-T946A/S949A (TS/AA) or PAM-1-T946D/S949D (TS/DD) (19) were maintained in a 5% $CO_2$ atomosphere in DMEM/F-12 supplemented with 100 units/ml penicillin, 100 μg/ml streptomycin, 10% fetal bovine serum, 10% NuSerum, Hepes buffer (final concentration, 25 mM) and 0.5 mg/ml G418 and passaged weekly.

### Biotinylation

Cell lines stably expressing PAM-1, PAM-1/TS/AA or PAM-1/TS/DD were incubated for 30 min in CSFM-air containing DMEM/F-12, 25 mM Hepes, pH 7.4 (no bicarbonate), 100 units/ml penicillin, 100 μg/ml streptomycin, insulin/transferrin/selenium and 0.1 mg/ml BSA. For surface biotinylation at 4°C, this step was carried out on ice and all solutions used were pre-chilled. Cells were rinsed with HSG buffer (15 mM Hepes, 120 mM NaCl, 2 mM $CaCl_2$, 4 mM KCl, 25 mM glucose, pH 7.5). Biotinylation was carried out with 1.25 mM Sulfo-NHS-LC-biotin (Pierce) dissolved in HSG buffer for 10 min at 37°C or 4°C. The reaction was quenched by replacing the buffer with CSFM-air with 2 mg/ml BSA for 5 min followed by rinsing in CSFM-air. During the chase, cells were incubated in CSFM-air supplemented with 1 mg/ml BSA. Secretion was stimulated by incubating cells in chase medium containing 1μM phorbol myristate acetate (PMA) and 2 mM $BaCl_2$ for 30 min (26). Cells were extracted immediately (Pulse) or after varying chase times in 20 mM NaTES, 10 mM mannitol, 1% Triton X-100, pH 7.4 (TMT) supplemented with protease inhibitors. Cell lysates and media were incubated with NeutrAvidin beads (Pierce) for 1 hr at 4C, washed twice with TMT and finally eluted by boiling in Laemmli sample buffer. All experiments were done in triplicate and controls (no biotin) were included each time. Samples were fractionated by SDS-PAGE, electroblotted onto PVDF membranes and probed with rabbit polyclonal antibody JH629 [rPAM-1(394–498), Exon A; 1:2000]. Quantification was performed on non-saturated signals acquired on a GeneGnome work station using Gene-Tools software (Syngene, Frederick, MD).

Unless mentioned differently, triplicate wells were analyzed in two separate experiments; error bars, SEM (n=6).

## Antibodies

The rabbit antisera used were JH629 [rPAM-1(394–498), Exon A (69)], JH2540 [P-T, P-S 946,9 (19)], JH1479 [TGN38(155-249) (21)], cation-independent mannose-6 phosphate receptor (I-5, a kind gift of Dr. Stefan Höning, University of Cologne) and Kathy [COOH-terminal ACTH (70)]). Monoclonal antibody 6E6 detects rPAM-1(898-976) (21). Monoclonal syntaxin 6 antibody was from BD Transduction Laboratories. Goat polyclonal EEA1 antibody (sc-6415) and chromogranin A antibody (sc-1488) were from Santa Cruz. Rat monoclonal Lamp1 antibody (1D4B) was from Developmental Studies Hybridoma Bank. Alexa Fluor 488 and 594 goat anti-rabbit, anti-mouse and anti-rat antibodies, donkey anti-goat and rabbit anti-goat antibodies were from Molecular Probes. Alexa Fluor 488 conjugated wheat germ agglutinin was from Molecular Probes, peroxidase conjugated wheat germ agglutinin (WGA-HRP) was from Sigma.

## Immunofluorescence

Cells grown on poly-L-lysine coated coverslips were fixed with methanol at -20°C or 4% paraformaldehyde at room temperature. Paraformaldehyde-fixed cells were permeabilized with 0.2% Triton-×100. Cells were incubated with primary antibody for 1 h at room temperature, then Alexa Fluor conjugated secondary antibody at 1:200 for 1 h at room temperature. Cells were viewed and photographed with a Leica TCS SP2 confocal microscope with a 65× or 100× oil immersion lens. For internalization studies, cells were rinsed with DMEM-Hepes containing 1mg/ml BSA, incubated in this medium with antibody JH629 (PAM) 1:2000 for 5 min at 37°C or 30 min at 4°C and then chased at 37°C in antibody free medium. The cells were then fixed and stained with Alexa Fluor secondary antibodies as above.

## Immunoelectron microscopy

Cells were fixed with 4% paraformaldehyde and 2% sucrose in 0.1 M phosphate buffer at room temperature, scraped, pelleted and embedded in gelatin. Polyvinylpyrrolidone/sucrose infiltrated specimens were sectioned at -120°C; sections were collected with methyl cellulose/sucrose, blocked with 1% fish skin gelatin (Sigma) and 1% BSA (Sigma) and incubated with antibody JH629 1:200 for 1 h followed by protein A-10 nm gold (University of Utrecht, Utrecht, Netherlands) for 1 h and embedded in uranyl acetate-methyl cellulose. For double staining with ACTH antibody, internalized PAM antibody was first detected with protein A-10 nm gold, the sections were fixed for 5 min with 1% glutaraldehyde to block interfering binding, then incubated with ACTH antibody Kathy 1:1000 followed by protein A-15 nm gold.

## Antibody internalization and electron microscopy

For immunoelectron microscopy in cryosections (Supplemental Table 1, Supplemental Figure 1), cells were incubated with antibody JH629 1:500 for 1 h, then fixed and processed for cryosections as above but incubated only with secondary antibody (protein A-10 nm gold). 10 nm gold particles were counted in systematically sampled micrographs (taken at 10,000 × magnification, enlarged 2.5 × for prints, 30 micrographs for each experiment, two experiments). Membrane associated gold particles were classified according to the membrane organelle and the result was expressed as percentage (± SEM of two separate experiments) of the total number of membrane associated gold particles per organelle. Golgi associated tubules were defined as tubules within 500 nm of the Golgi stack. The relative surface area occupied by membrane organelles was then determined from the same prints by point counting (71) and the result was expressed as gold particles/$\mu m^2$ organelle profile. To give a labeling index, labeling over mitochondria was taken as a measure of non-specific labeling.

For pre-embedding labeling at the electron microscope level, cells were incubated with antibody JH629 1:500 in DMEM-Hepes-1mg/ml BSA for 10 min at 37°C and chased in culture medium at 37°C. The cells were fixed with PLP (2% formaldehyde, 0.01 M periodate and 0.075 M lysine-HCl in 0.075 M phosphate buffer, pH 7.4) for 2 h at room temperature. Cells were permeabilized with 0.01% saponin (Sigma) and incubated for 1 h with 1.4 nm gold particle-conjugated Fab fragments against rabbit immunoglobulin G (Nanoprobes). Nanogold was silver enhanced with an HQ Silver kit (Nanoprobes) for 0.5 to 2 min and gold toned with 0.05% gold chloride. Cells were then post-fixed with 1% osmium tetroxide and 1.5% potassium ferrocyanide, dehydrated and embedded in Epon. Sections were poststained with uranyl acetate and lead citrate.

For colloidal gold labeling at the electron microscope level, cells were incubated with antibody JH629 1:250 in DMEM-Hepes-BSA for 1 h at 4°C, rinsed with DMEM-Hepes-BSA at 4°C, incubated in DMEM-Hepes with protein A-15 nm colloidal gold (University of Utrecht, Utrecht, Netherlands) at the concentration suggested for immunolabeling by the provider (1:60-75) for 1 h at 4°C, rinsed in DMEM-Hepes at 4°C and then chased in culture medium at 37°C. Control cells were incubated with protein A-colloidal gold only. After the chase, cells were fixed with 2.5% glutaraldehyde and 2% sucrose in 0.1 M sodium cacodylate buffer and osmificated, dehydrated end embedded in Epon as above. For classification of gold particle containing endosomal structures (Figs. 7,8) sections were systematically scanned for gold label to give 40 labeled cells, 400-800 gold particles for each group in each experiment

For uptake of cationized ferritin, cells were incubated with 0.5 mg/ml cationized ferritin (Sigma) for 1 h at 37°C, fixed with 2.5% glutaraldehyde and processed as above.

For WGA-HRP uptake, cells were incubated with 30 μg/ml WGA-HRP (Sigma) on ice for 1 h, chased in culture medium at 20°C or 37°C, fixed with 1.5% glutaraldehyde in 0.1 M phosphate buffer, incubated with 0.25 mg/ml diaminobenzidine in 0.05 M Tris-HCl buffer pH 7.6 and 1.8 μl hydrogen peroxide for 10 min on ice, then osmicated, dehydrated and embedded in Epon as above.

For time-lapse analysis of PAM and WGA uptake the cells were incubated with antibody JH629 1:1000 in DMEM-Hepes-BSA for 30 min on ice, rinsed, incubated with Alexa 594 labeled anti-rabbit IgG Fab fragment (Zenon labelling reagent, Molecular Probes) 1:20 and 1.5 μg/ml WGA-Alexa 488 (Molecular Probes) for 30 min on ice, rinsed and then viewed and photographed in DMEM-Hepes-BSA-1% insulin-transferrin-selenium (Gibco) with a Leica TCS SP2 confocal microscope provided with a 37C temperature chamber, either directly (Supplemental movie 1) or after incubation for 2 h at 20°C (Supplemental movie 2). Movies were generated with a 63× objective, movie frames were collected at 60 sec intervals. No uptake was seen when cells were labelled with only secondary antibody.

## Supplementary Material

Refer to Web version on PubMed Central for supplementary material.

## Acknowledgments

Supported by the Liv och Hälsa Foundation, the Magnus Ehrnrooth Foundation, the Perklén Foundation and by the National Institutes of Health (DK32949). We thank the Electron Microscopy unit of the Institute of Biotechnology, University of Helsinki for providing laboratory facilities.

## References


1. Pelletier G. Secretion and uptake of peroxidase by rat adenohypophyseal cells. J Ultrastruct Res 1973;43:445–459. [PubMed: 4352596]
2. Farquhar MG. Recovery of surface membrane in anterior pituitary cells. J Cell Biol 1978;77:R35–R42. [PubMed: 567224]
3. Farquhar, MG. Ciba Foundation Symposium. Vol. 92. Pitman Books Ltd.; London: 1982. Membrane recycling in secretory cells: pathway to the Golgi complex; p. 157-183.
4. Romagnoli P, Herzog V. Reinternalization of secretory proteins during membrane recycling in rat pancreatic acinar cells. Eur J Cell Biol 1987;44:167–175. [PubMed: 3500858]
5. Patzak A, Winkler H. Exocytotic exposure and recycling of membrane antigens of chromaffin granules: ultrastructural evaluation after immunolabeling. J Cell Biol 1986;102:510–515. [PubMed: 3080437]
6. Milgram SL, Mains RE, Eipper BA. COOH-terminal signals mediate the trafficking of a peptide processing enzyme in endocrine cells. J Cell Biol 1993;121:23–36. [PubMed: 8458870]
7. Hurtley SM. Recycling of a secretory granule membrane protein after stimulated secretion. J Cell Sci 1993;106:649–656. [PubMed: 8282769]
8. Solimena M, Dirkx R, Hermel JM, Pleasic-Williams S, Shapiro JA, Caron L, Rabin DU. ICA 512, an autoantigen of type I diabetes, is an intrinsic membrane protein of neurosecretory granules. EMBO J 1996;15:2102–2114. [PubMed: 8641276]
9. Wasmeier C, Burgos PV, Trudeau T, Davidson HW, Hutton JC. An extended tyrosine-targeting motif for endocytosis and recycling of the dense-core vesicle membrane protein phogrin. Traffic 2005;6:474–487. [PubMed: 15882444]
10. Subramaniam M, Koedam JA, Wagner DD. Divergent fates of P- and E-selectins after their expression on the plasma membrane. Mol Biol Cell 1993;4:791–801. [PubMed: 7694691]
11. Trajkovski M, Mziaut H, Altkrüger A, Ouwndijk J, Knoch KP, Müller S, Solimena M. Nuclear translocation of an ICA512 cytosolic fragment couples granule exocytosis and insulin expression in β-cells. J Cell Biol 2004;167:1063–1074. [PubMed: 15596545]
12. Rajagopal C, Stone KL, Francone VP, Mains RE, Eipper BA. Secretory granule to the nucleus: role of a multiply phosphorylated intrinsically unstructured domain. J Biol Chem 2009;284:25723–25734. [PubMed: 19635792]
13. Piper CR, Katzmann DJ. Biogenesis and function of multivesicular bodies. Annu Rev Cell Dev Biol 2007;23:519–547. [PubMed: 17506697]
14. Bonifacino JS, Rojas R. Retrograde transport from endosomes to the trans-Golgi network. Nat Rev Cell Mol Biol 2006;7:568–579.
15. Saftig P, Klumperman J. Lysosome biogenesis and lysosomal membrane proteins: trafficking meets function. Nat Rev Mol Cell Biol 2009;10:623–635. [PubMed: 19672277]
16. Eipper BA, Milgram SL, Husten EJ, Yun HY, Mains RE. Peptidylglycine α-amidating monooxygenase: a multifunctional protein with catalytic, processing and routing domains. Protein Sci 1993;2:489–497. [PubMed: 8518727]
17. Alam MR, Caldwell BD, Johnson RC, Darlington DN, Mains RE, Eipper BA. Novel proteins that interact with the COOH-terminal cytosolic routing determinants of an integral membrane peptide-processing enzyme. J Biol Chem 1996;271:28636–28640. [PubMed: 8910496]
18. Steveson TC, Keutmann HT, Mains RE, Eipper BA. Phosphorylation of cytosolic domain $Ser^{937}$ affects both biosynthetic and endocytic trafficking of peptidylglycine α-amidating monooxygenase. J Biol Chem 1999;274:21128–21138. [PubMed: 10409666]
19. Steveson TC, Zhao GC, Keutmann HT, Mains RE, Eipper BA. Access of a membrane protein to secretory granules is facilitated by phosphorylation. J Biol Chem 2001;276:40326–40337. [PubMed: 11524414]
20. Milgram SL, Johnson RC, Mains RE. Expression of individual forms of peptidylglycine α-amidating monooxygenase in AtT-20 cells: endoproteolytic processing and routing to secretory granules. J Cell Biol 1992;117:717–728. [PubMed: 1577852]
21. Milgram SL, Kho ST, Martin GV, Mains RE, Eipper BA. Localization of integral membrane peptidylgycine α-amidating monooxygenase in neuroendocrine cells. J Cell Sci 1997;110:695–706. [PubMed: 9099944]

22. Alam MR, Steveson TC, Johnson RC, Bäck N, Abraham B, Mains RE, Eipper BA. Signaling mediated by the cytosolic domain of peptidylglycine α-amidating monooxygenase. Mol Biol Cell 2001;12:629–644. [PubMed: 11251076]
23. Wendler F, Tooze S. Syntaxin 6: The promiscuous behavior of a SNARE protein. Traffic 2001;2:606–611. [PubMed: 11555414]
24. Kuliawat R, Kalinina E, Boch J, Fricker L, McGraw TE, Kim SR, Zhong J, Scheller R, Arvan P. Syntaxin-6 SNARE involvement in secretory and endocytic pathways of cultured pancreatic β-cells. Mol Biol Cell 2004;15:1690–1701. [PubMed: 14742717]
25. Pérez-Victoria FJ, Bonifacino JS. Dual roles of the mammalian GARP complex in tethering and SNARE complex assembly at the trans-Golgi network. Mol Cell Biol 2009;29:5251–5263. [PubMed: 19620288]
26. Ferraro F, Eipper BA, Mains RE. Retrieval and reuse of pituitary secretory granule proteins. J Biol Chem 2005;280:25424–25435. [PubMed: 15905171]
27. Mains RE, Eipper BA. Coordinate, equimolar secretion of smaller peptide products derived from pro-ACTH/endorphin by mouse pituitary tumosr cells. J Cell Biol 1981;89:21–28. [PubMed: 6262331]
28. Tooze J, Tooze SA. Clathrin-coated vesicular transport of secretory proteins during the formation of ACTH-containing secretory granules in AtT20 cells. J Cell Biol 1986;103:839–850. [PubMed: 3017997]
29. Van Dyke RW. Proton pump-generated electrochemical gradients in rat liver multivesicular bodies. J Biol Chem 1988;263:2603–2611. [PubMed: 2963813]
30. Falguiéres T, Luyet PP, Bissig C, Scott CC, Velluz MC, Gruenberg J. In vitro budding of intralumenal vesicles into late endosomes is regulated by Alix and Tsg101. Mol Biol Cell 2008;19:4942–4955. [PubMed: 18768755]
31. Tooze J, Hollinshead M. Tubular early endosomal networks in AtT20 and other cells. J Cell Biol 1991;115:635–653. [PubMed: 1918157]
32. Caldwell BD, Darlington DN, Penzes P, Johnson RC, Eipper BA, Mains RE. The novel kinase peptidylglycine α-amidating monooxygenase cytosolic interactor protein 2 interacts with the cytosolic routing determinants of the peptide processing enzyme peptidylglycine α-amidating monooxygenase. J Biol Chem 1999;274:34646–34656. [PubMed: 10574929]
33. Blagoveshchenskaya AD, Hewitt EW, Cutler DF. A balance of opposing signals within the cytoplasmic tail controls the lysosomal targeting of P-selectin. J Biol Chem 1998;273:27896–2790. [PubMed: 9774401]
34. Milgram SL, Eipper BA, Mains RE. Differential trafficking of soluble and integral membrane secretory granule-associated proteins. J Cell Biol 1994;124:33–41. [PubMed: 8294504]
35. De M, Ciccotosto GD, Mains RE, Eipper BA. Trafficking of a secretory granule membrane protein is sensitive to copper. J Biol Chem 2007;282:23362–23371. [PubMed: 17562710]
36. Willingham MC, Hanover JA, Dickson RB, Pastan I. Morphologic characterization of the pathway of transferring endocytosis and recycling in human KB cells. Proc Natl Acad Sci USA 1984;81:175–179. [PubMed: 6141558]
37. Griffiths, G. Fine structure immunocytochemistry. Springer-Verlag; Berlin: 1993.
38. Bright NA, Reaves BJ, Mullock BM, Luzio JP. Dense core lysosomes can fuse with late endosomes and are re-formed from the resultant hybrid organelles. J Cell Sci 1997;110:2027–2040. [PubMed: 9378754]
39. Katzmann DJ, Odorizzi G, Emr SD. Receptor downregulation and multivesicular- body sorting. Nat Rev Mol Cell Biol 2002;3:893–905. [PubMed: 12461556]
40. Williams RL, Urbé S. The emerging shape of the ESCRT machinery. Nat Rev Mol Cell Biol 2007;8:355–368. [PubMed: 17450176]
41. Theos AC, Truschei ST, Tenza D, Hurbain I, Harper DC, Berson JF, Thomas PC, Raposo G, Marks MS. A lumenal domain-dependent pathway for sorting to intralumenal vesicles of multivesicular endosomes involved in organelle morphogenesis. Dev Cell 2006;10:343–354. [PubMed: 16516837]
42. Hislop JN, Marley A, von Zastrow M. Role of mammalian vacuolar protein-sorting proteins in endocytic trafficking of a non-ubiquinated G protein-coupled receptor to lysosomes. J Biol Chem 2004;279:22522–22531. [PubMed: 15024011]

43. Gullapalli A, Wolfe BL, Griffin CT, Magnuson T, Trejo J. An essential role for SNX1 in lysosomal sorting of protease-activated receptor-1: evidence for retromer-, HRS-, and Tsg101-independent functions of sorting nexins. Mol Biol Cell 2006;17:1228–1238. [PubMed: 16407403]
44. Gillooly DJ, Morrow IC, Lindsay M, Gould R, Bryant NJ, Gaullier JM, Parton RG, Stenmark H. Localization of phosphatidylinositol 3-phosphate in yeast and mammalian cells. EMBO J 2000;19:4577–4588. [PubMed: 10970851]
45. White IJ, Bailey LM, Aghakhani MR, Moss SE, Futter CE. EGF stimulates annexin 1-dependent inward vesiculation in a multivesicular endosome subpopulation. EMBO J 2006;25:1–12. [PubMed: 16052208]
46. Murk JL, Stoorvogel W, Kleijmeer MJ, Geuze HJ. The plasticity of multivesicular bodies and the regulation of antigen presentation. Cell Dev Biol 2002;13:303–311.
47. Kleijmeer M, Ramm G, Schuurhuis D, Griffith J, Rescigno M, Riccicardi-Castagnoli P, Rudensky AY, Ossendorp F, Melief CJM, Stoorvogel W, Geuze HJ. Reorganization of multivesicular bodies regulates MHC class II antigen presentation by dendritic cells. J Cell Biol 2001;155:53–63. [PubMed: 11581285]
48. Abrami L, Lindsay M, Parton RG, Leppla SH, van der Goot FG. Membrane insertion of anthrax protective antigen and cytoplasmic delivery of lethal factor occur at different stages of the endocytotic pathway. J Cell Biol 2004;166:645–651. [PubMed: 15337774]
49. Le Blanc I, Luyet PP, Pons V, Ferguson C, Emans N, Petiot A, Mayran N, Demaurex N, Fauré J, Sadoul R, Parton RG, Gruenberg J. Endosome-to-cytosol transport of viral nucleocapsids. Nat Cell Biol 2005;7:653–664. [PubMed: 15951806]
50. Gonzales-Gaitan M. Signal dispersal and transduction through the endocytic pathway. Nat Rev Mol Cell Biol 2003;4:213–224. [PubMed: 12612640]
51. Miaczynka M, Pelkmans L, Zerial M. Not just a sink: endosomes in control of signal transduction. Curr Opin Cell Biol 2004;16:400–406. [PubMed: 15261672]
52. Hisata S, Sakisaka T, Baba T, Yamada T, Aoiki K, Matsuda M, Takai Y. Rap1-PDZ-GEF1 interacts with a neurotrophin receptor at late endosomes, leading to sustained activation of Rap1 and ERK and neurite outgrowth. J Cell Biol 2007;178:843–860. [PubMed: 17724123]
53. Yap CC, Wisco D, Kujla P, Lasiecka ZM, Cannon JT, Chang MC, Hirling H, Klumperman J, Winckler B. The somatodendritic endosomal regulator NEEP21 facilitates axonal targeting of L1/NgCAM. J Cell Biol 2008;180:827–842. [PubMed: 18299352]
54. Escola JM, Kleijmeer M, Stoorvogel W, Griffith JM, Yoshie O, Geuze HJ. Selective enrichment of tetraspan proteins on the internal vesicles of multivesicular endosomes and on exosomes secreted by human B-lymphocytes. J Biol Chem 1998;273:20121–20127. [PubMed: 9685355]
55. Kobayashi TK, Vischer UM, Rosnoblet C, Levrand C, Lindsay M, Parton RG, Kruithof EKO, Gruenberg J. The tetraspanin CD63/lamp3 cycles between endocytic and secretory compartments in human endothelial cells. Mol Biol Cell 2000;11:1829–1843. [PubMed: 10793155]
56. Möbius W, van Donselaar E, Ohno-Iwashita Y, Shimada Y, Heijnen HFG, Geuze HJ. Recycling compartments and the internal vesicles of multivesicular bodies harbor most of the cholesterol found in the endocytic pathway. Traffic 2003;4:2222–231.
57. Falguières T, Luyet PP, Gruenberg J. Molecular assemblies and membrane domains in multivesicular endosome dynamics. Exp Cell Res 2009;315:1567–1573. [PubMed: 19133258]
58. Tomiyama Y, Waguri S, Kanamori S, Kametaka S, Wakasugi M, Shibata M, Ebisu S, Uchiyama Y. Early-phase redistribution of the cation-independent mannose 6-phosphate receptor by U18666A treatment in HeLa cells. Cell Tissue Res 2004;317:253–264. [PubMed: 15322907]
59. Bell-Parikh LC, Eipper BA, Mains RE. Response of an integral granule membrane protein to changes in pH. J Biol Chem 2001;276:29854–29863. [PubMed: 11395514]
60. Ehlers MRW, Riordan JF. Membrane proteins with soluble counterparts: role of proteolysis in the release of transmembrane proteins. Biochemistry 1991;30:10065–10074. [PubMed: 1931937]
61. Seals DF, Courtneidge SA. The ADAMs family of metalloproteases: multidomain proteins with multiple functions. Genes & Dev 2003;17:7–30. [PubMed: 12514095]
62. Mathews PM, Guerra CB, Jiang Y, Grbovic OM, Kao BH, Schmidt SD, Dinakar R, Mercken M, Hille-Rehfeld A, Rohrer J, Mehta P, Cataldo AM, Nixon PA. Alzheimer's disease-related

overexpression of the cation-dependent mannose 6-phosphate receptor increases Aβ secretion. J Biol Chem 2002;277:5299–5307. [PubMed: 11551970]

63. Zhang M, Haapasalo A, Kim DY, Ingano LAM, Petingell WH, Kovacs DM. Presenilin/γ-secretase activity regulates protein clearance from the endocytic recycling compartment. FASEB J 2006;20:E271–E280.
64. Takahashi RH, Milner TA, Li F, Nam EE, Edgar MA, Yamaguchi H, Beal MF, Xu H, Greengard P, Gouras GK. Intraneuronal Alzheimer Aβ42 accumulates in multivesicular bodies and is associated with synaptic pathology. Am J Pathol 2002;161:1869–1879. [PubMed: 12414533]
65. Rajendran L, Honsho M, Zahn TR, Keller P, Geiger KD, Verkade P, Simons K. Alzheimer's disease β-amyloid peptides are released in association with exosomes. Proc Natl Acad Sci USA 2006;103:11172–11177. [PubMed: 16837572]
66. Sahagian GG. The mannose 6-phosphate receptor: function, biosynthesis and translocation. Biol Cell 1984;51:207–214. [PubMed: 6240303]
67. Clairmont KB, Czech MP. Extracellular release as the major degradative pathway of the insulin-like growth factor II/mannose 6-phosphate receptor. J Biol Chem 1991;266:12131–12134. [PubMed: 1648081]
68. Rohrer J, Schweizer A, Johnson KF, Kornfeld S. A determinant in the cytoplasmic tail of the cation-dependent mannose 6-phosphate receptor prevents trafficking to lysosomes. J Cell Biol 1995;130:1297–1306. [PubMed: 7559753]
69. Yun HY, Milgram SL, Keutmann HT, Eipper BA. Phosphorylation of the cytosolic domain of peptidylglycine alpha-amidating monooxygenase. J Biol Chem 1995;270:30075–30083. [PubMed: 8530412]
70. Schnabel E, Mains RE, Farquhar MG. Proteolytic processing of pro-ACTH/endorphin begins in the Golgi complex of pituitary corticotropes and AtT-20 cells. Mol Endocrinol 1989;3:1223–1235. [PubMed: 2550814]
71. Weibel, ER. Stereological methods Vil 1 Practical methods for biological morphometry. Academic Press; London: 1979.

## Abbreviations

| | |
|---|---|
| SG | secretory granule |
| MVB | multivesicular body |
| ILV | intralumenal vesicle |
| TGN | trans-Golgi network |
| PAM | peptidylglycine α-amidating monooxygenase |
| PHM | peptidylglycine α-hydroxylating monooxygenase |
| PAL | peptidyl-α-hydroxyglycine α-amidating lyase |

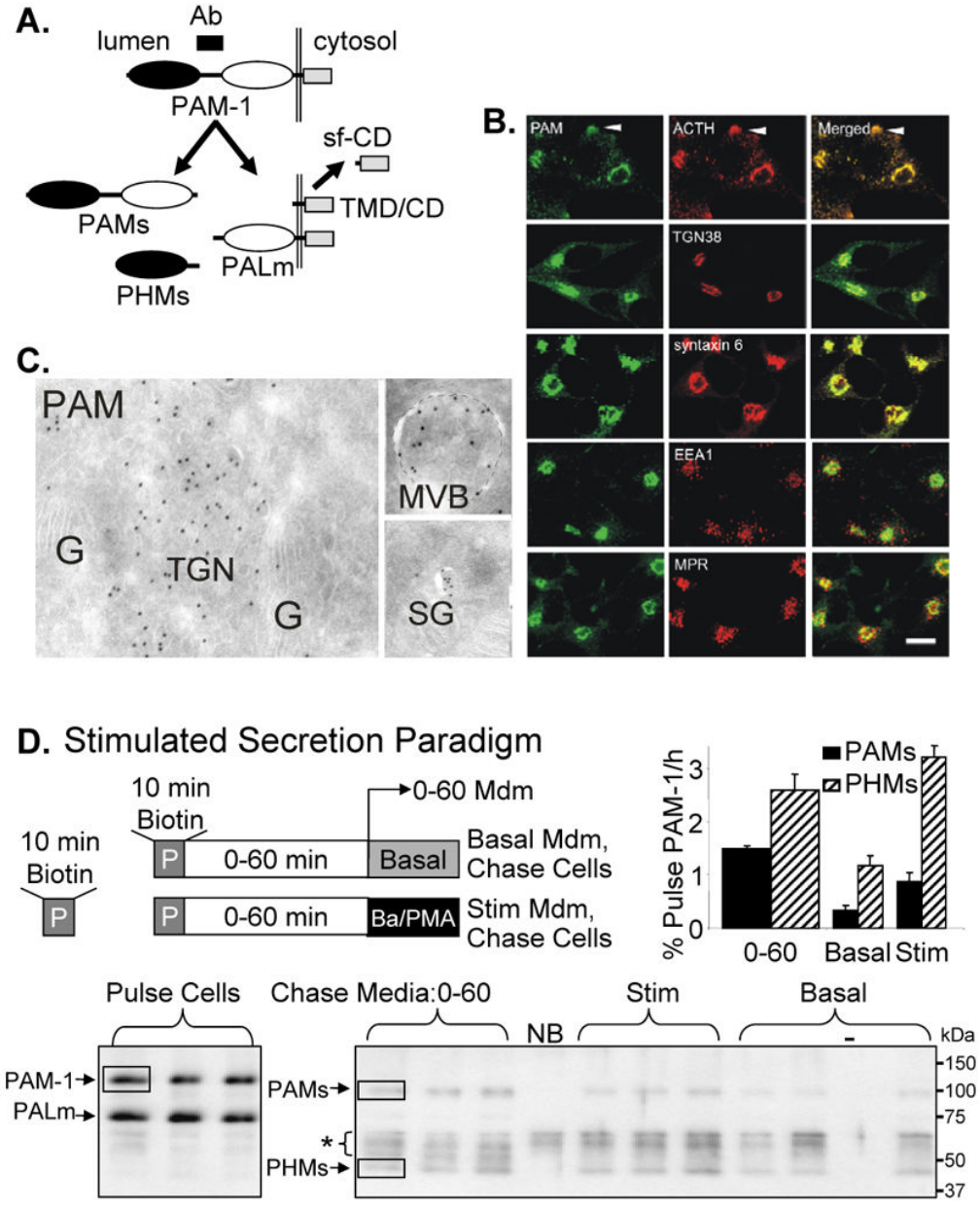


**Figure 1. Cell surface PAM-1 enters regulated granules**

(**A**) The PAM-1 epitope recognized by the antibody used for these studies is indicated (Ab). Cleavage to PHMs and PALm (both of which are detected by this antibody) occurs in SGs; PAMs, TMD/CD and a soluble fragment of the cytosolic domain (sf-CD) are shown. (**B**) The steady state distribution of PAM was compared to that of ACTH, TGN38, syntaxin 6, EEA1 and CI-MPR. Scale bar, 10 μm (**C**) EM detection of PAM in cryosections using PAM antibody followed by protein A-10 nm gold shows PAM in the TGN, in MVB intralumenal vesicles and in SGs; G = Golgi cisternae; TGN, trans-Golgi network. Scale bar, 200 nm. (**D**) The paradigm used to evaluate the return of PAM-1 biotinylated on the cell surface to SGs is illustrated; nine wells of PAM-1 AtT-20 cells were exposed to membrane impermeant activated biotin (Methods) for 10 min at 37°C; after the reaction was quenched, cells were harvested immediately (Pulse; n = 3) or chased for 60 min. After 0-60 min, medium was harvested (n =

6), triplicate wells were incubated in Basal or Stim (2 mM $BaCl_2$, 1 μM phorbol myristate acetate; PMA) media for 30 min. Media and Cells were harvested for analysis. Biotinylated PAM proteins recovered from Cells and Media were visualized by Western blot; molecular weight marker mobilities are shown to the right. NB, no biotin control and -, no sample in lane. Boxes show typical regions quantified and asterisk marks nonspecific background. Medium lanes received 16 times more sample than Pulse. Quantification: data for secreted biotinylated PAM proteins are expressed relative to the amount of biotinylated PAM-1 in cell lysates after the Pulse.

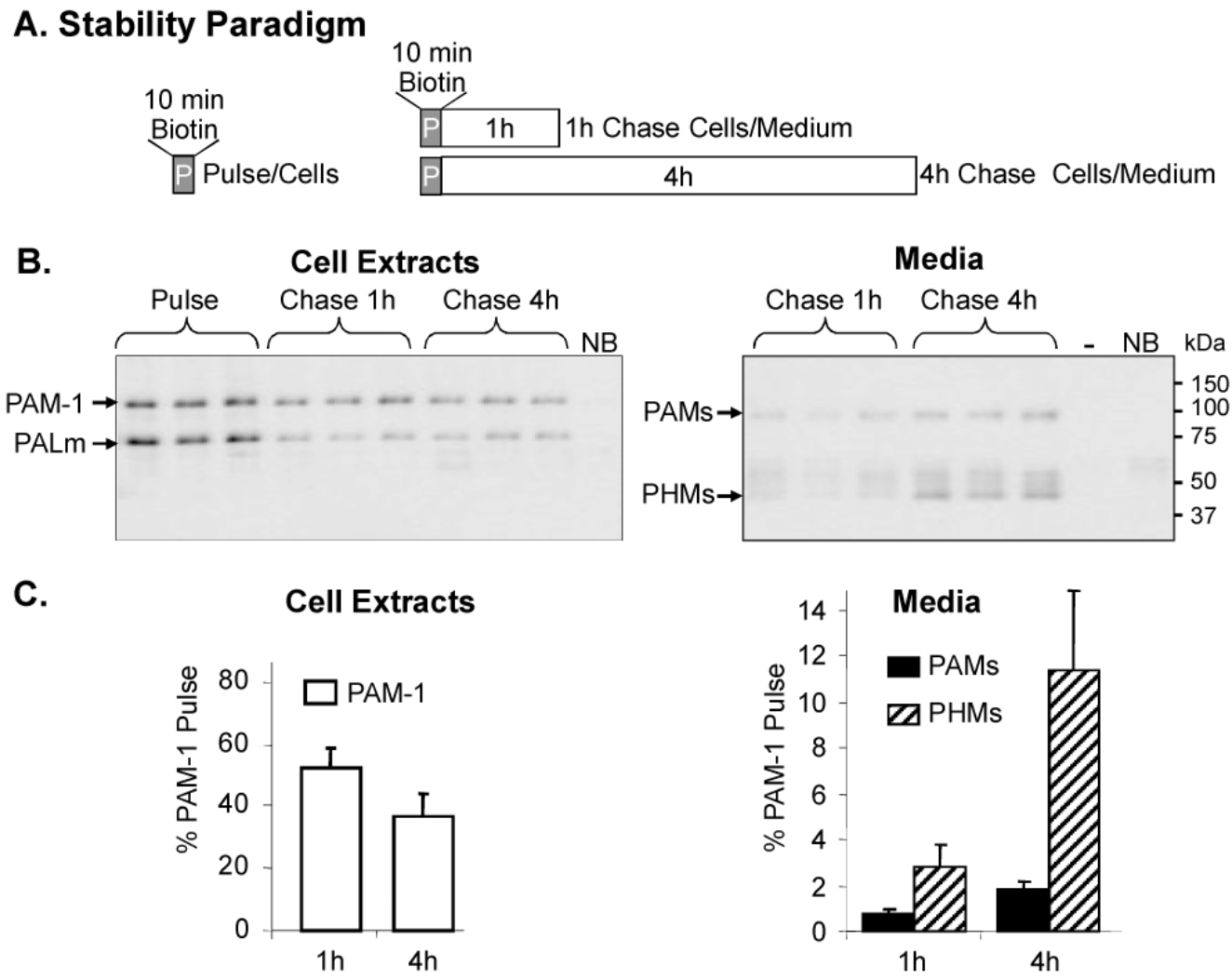


**Figure 2. Stability of PAM-1 in the endocytic pathway**

(**A**) Schematic of biotinylation paradigm used to assess stability. Nine wells of PAM-1 AtT-20 cells were biotinylated at 37°C for 10 min; after the reaction was quenched, cells were harvested (Pulse, n = 3) or chased in basal medium for 1 h or 4 h; at the end of each Chase, Cells and Media were harvested for analysis of biotinylated PAM. (**B**) Cell extracts (left panel) and chase media (right) were analyzed; Media lanes contained 16 times more sample than Pulse. (**C**) Recovery of biotinylated PAM-1 (left) in Cell Extracts and biotinylated PAMs/PHMs (right panel) in Media.

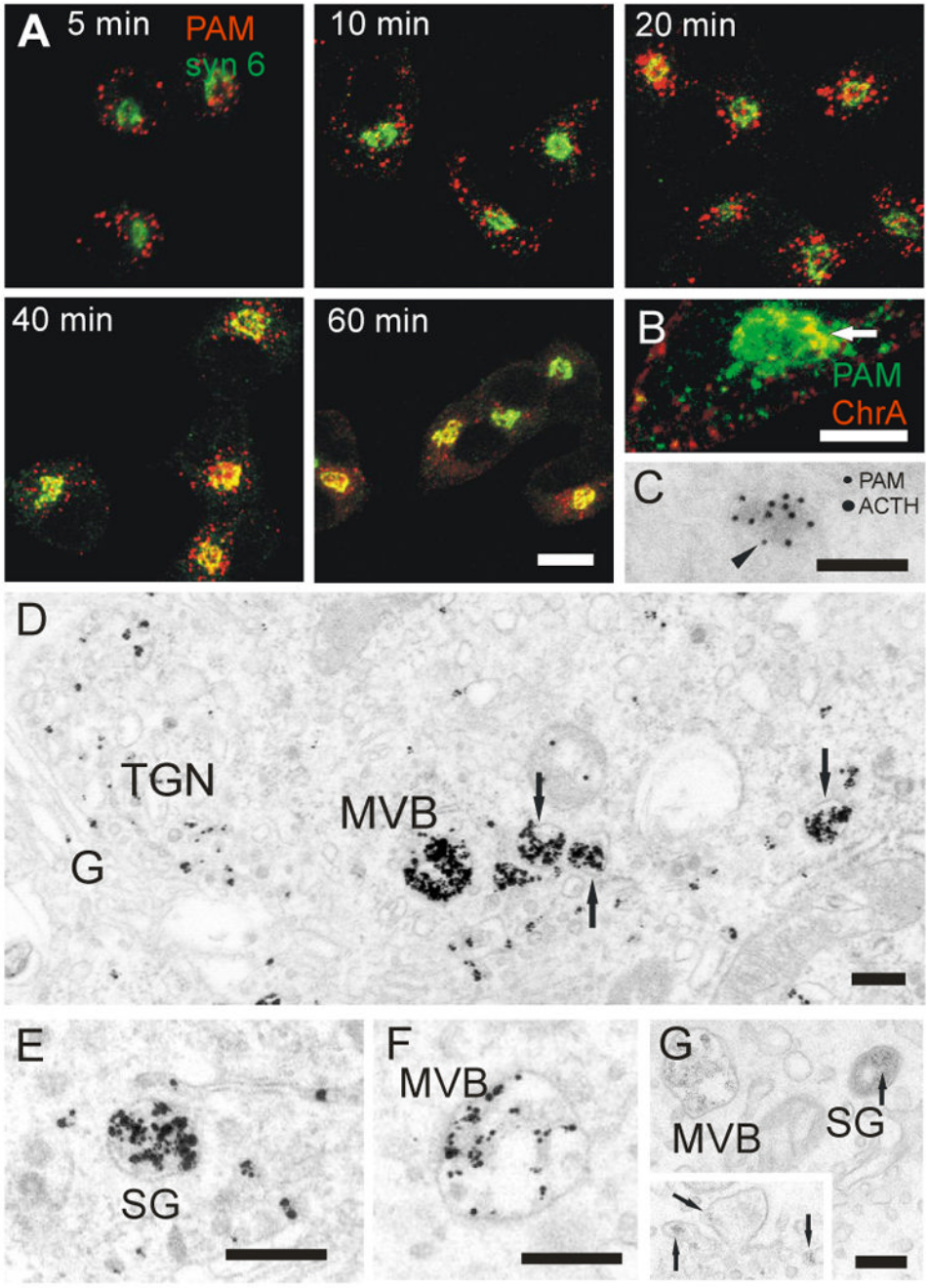


**Figure 3. Timing of PAM antibody uptake**

(**A**) AtT-20 PAM-1 cells were allowed to internalize PAM antibody (red) for 5-60 min. Immunostaining for syntaxin 6 (green) identifies the TGN, immature SGs and endosomes (23-25), compartments occupied by PAM at steady state. Colocalization of internalized antibody with syntaxin 6 was first detectable at 10 min, and increased markedly at 20 and 40 min; scale bar, 10 μm. (**B**) Focal colocalization of PAM antibody internalized for 40 min (green) and chromogranin A (red) in the TGN. Scale bar, 10 μm. (**C**) PAM-1 antibody was internalized for 1 h; cells were then fixed and prepared for cryosectioning. PAM-1 antibody was detected with 10 nm protein A-gold (arrowhead). After blocking, the sections were incubated with ACTH antibody that was detected with 15 nm protein A-gold. Scale bar, 200 nm. (**D-F)** PAM

antibody internalized for 60 min at 37°C was visualized by pre-embedding staining. Label was seen in MVBs, in the TGN and in immature SGs (arrows). An MVB (**F**) is shown after more mild silver intensification of the gold label, allowing better resolution of the ultrastructure and distinction from immature SGs. Scale bars, 200 nm. (**G**) Cationized ferritin internalized for 1 h is seen as a fine granular label in MVBs and immature SGs. The insert shows cationized ferritin in the TGN and in the membrane enclosing an early condensation of secretory material in the TGN (arrows). Scale bar, 200 nm.

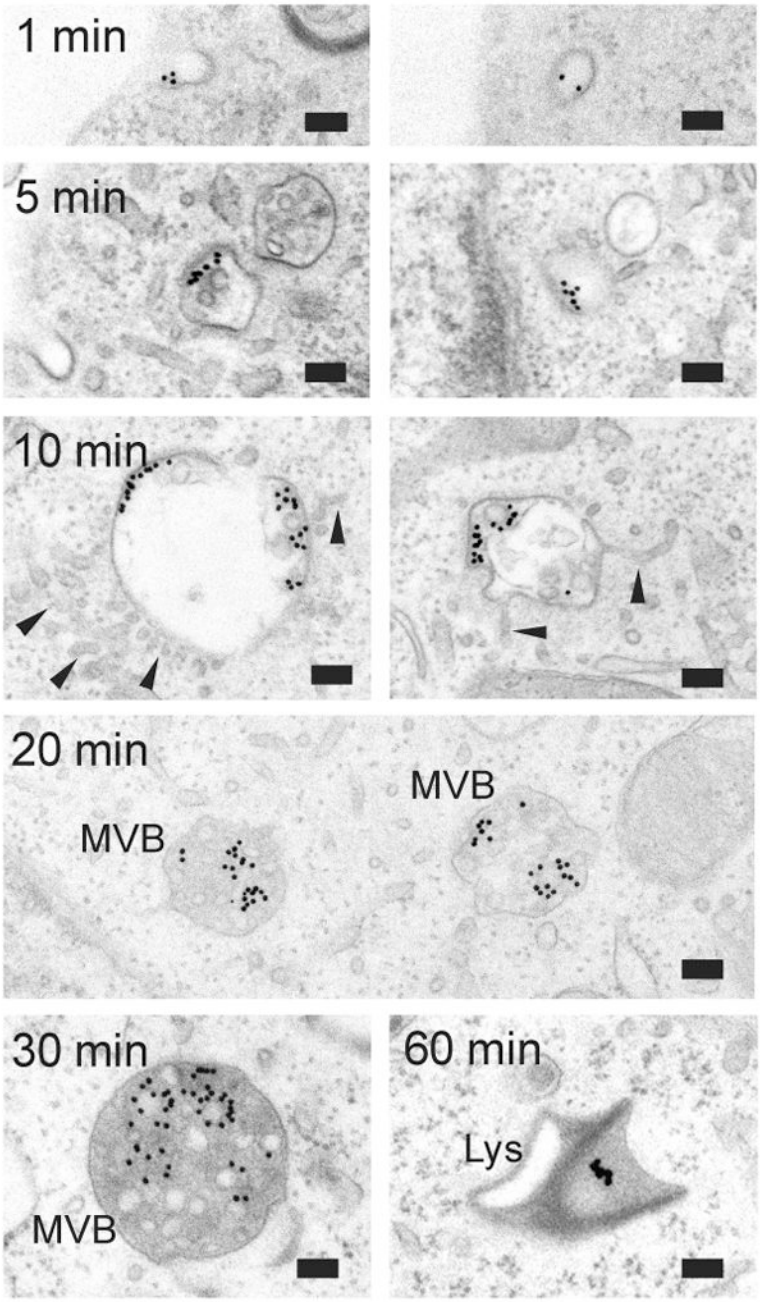


**Figure 4. Internalization of PAM-1 antibody/colloidal gold complex**

After 1 min at 37°C, PAM Ab/protein-gold complexes were in coated plasma membrane invaginations or vesicles. After 5 or 10 min, label was in subdomains of early endosomal membranes; label was excluded from tubular extensions (arrowheads). After 20 and 30 min, PAM Ab/proteinA-gold complexes were on internal vesicles of MVBs. Aggregated gold particles were detected in lysosomes after 20-60 min. Scale bar, light microscopy 2.5 μm; electron microscopy 100 nm.

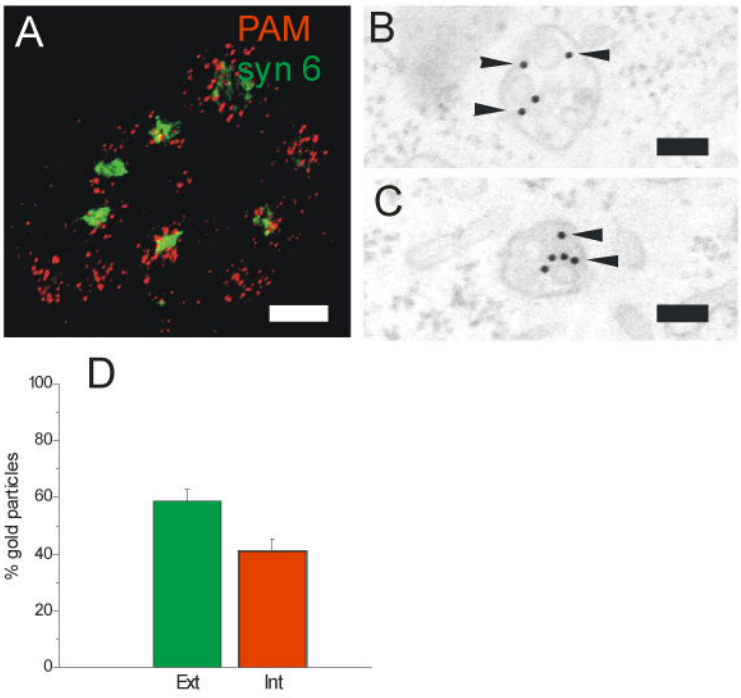


**Figure 5. PAM-1 antibody uptake for 1 h at 20°C**

(**A**) After uptake for 1 h at 20°C, PAM-1/Ab complexes (red) accumulated in rounded endosomes of varying size; no label was seen in the TGN (syntaxin 6 staining, green, compare to Fig. 3A). (**B,C**) Using PAM Ab/protein A-gold complexes under the same conditions, these structures were identified as MVBs; the proportion of gold particles associated with the limiting (Ext) versus internal (Int) vesicle membrane was quantified (± SEM of two separate experiments) (**D**). Scale bars: **A**, 5 μm; **B,C**, 100 nm.

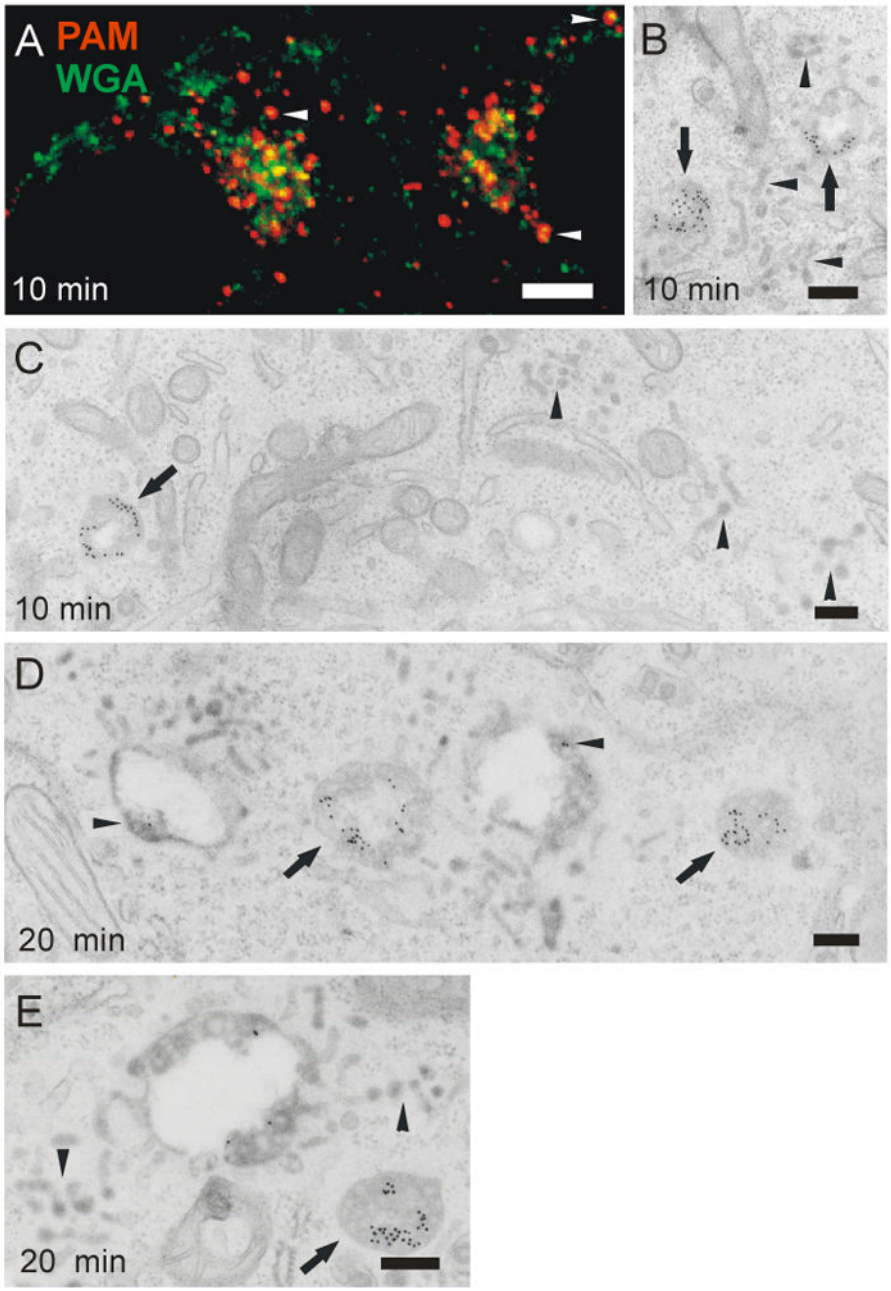


**Figure 6. A-D. Differences in the uptake of WGA and PAM antibody**

(**A**) Partial overlap of WGA-Alexa 488 (green) and PAM antibody (red) in peripheral endosomes (arrowhead) and in the trans-Golgi area after 10 min of uptake. Scale bar, 2.5 μm. (**B,C**) Electron microscopy of 10 min uptake shows PAM Ab/proteinA-gold complexes in round endosomes (arrows) and WGA-HRP in tubules closer to the cell membrane (arrowheads). Some endosomes contain both markers in their vacuolar part, with WGA-HRP in the extending tubules (arrows in **B**). (**D,E**) After 20 min of uptake, PAM Ab/proteinA-gold complexes are concentrated on intralumenal vesicles of MVBs devoid of WGA (arrows). Few gold complexes are seen on the intralumenal vesicles of WGA-containing endosomes (arrowheads). Scale bars, 200 nm.

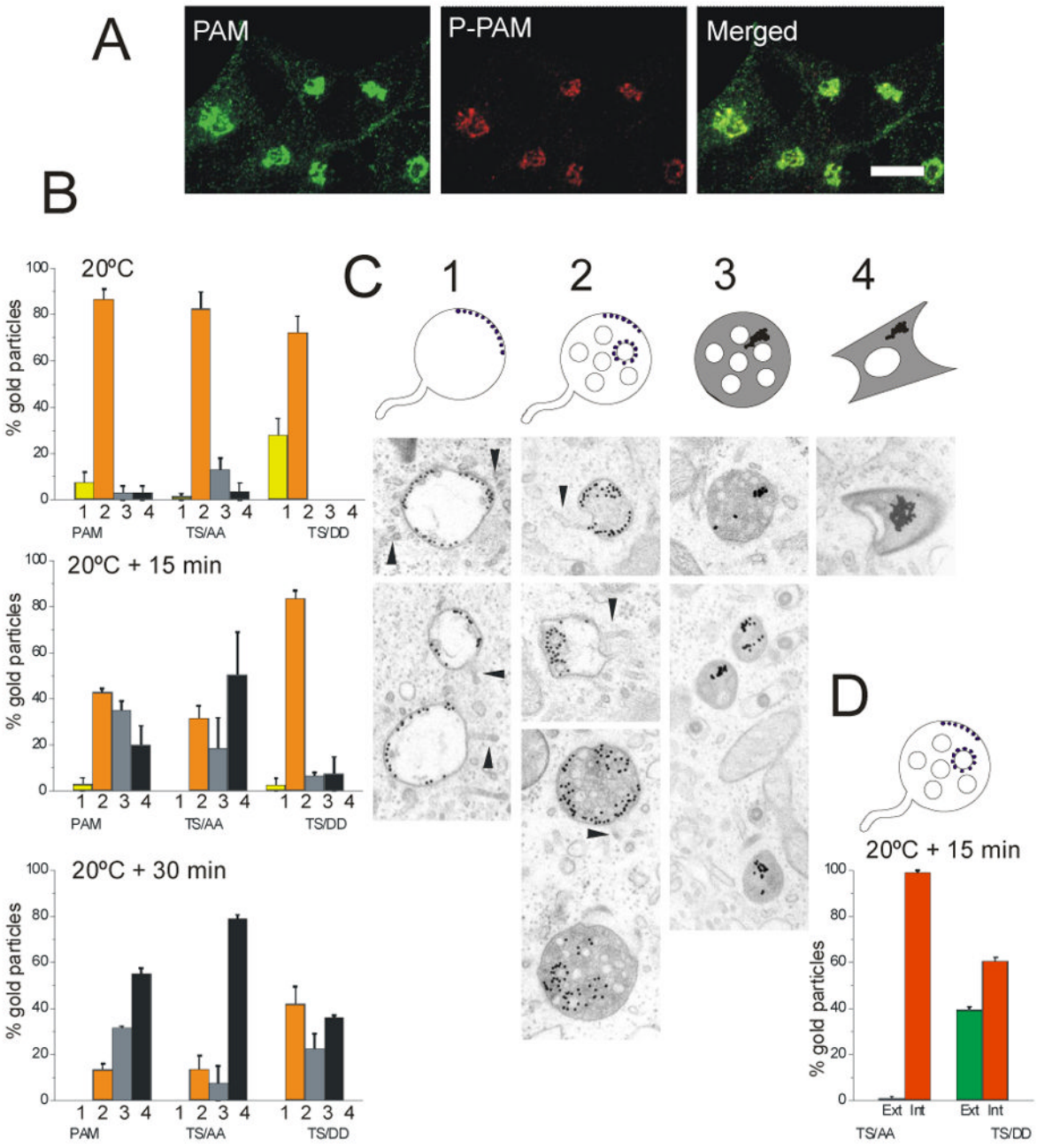


**Figure 7. Mutations affecting PAM cytosolic domain phosphorylation control entry into ILVs**

(**A**) PAM-1 AtT-20 cells were visualized using polyclonal antibody specific for phosphorylation at $Ser^{949}$ (red, P-PAM) and monoclonal antibody to the PAM cytosolic domain (green). Scale bar, 10 μm. (**B**) AtT-20 cells expressing PAM-1, PAM-1/TS/AA or PAM-1/TS/DD were allowed to internalize PAM Ab/Protein A-gold complex for 1 h at 20°C and fixed or rinsed and incubated at 37°C for 15 or 30 min; error bars, ± SEM of two separate experiments. Organelles containing gold particles were classified as early endosomal structures (1, yellow), MVBs (2, orange), MVBs containing aggregated gold particles (3, grey) and lysosomes containing aggregated gold particles (4, black). (**C**) Examples of each category are shown - arrowheads indicate tubules extending from early endosomes and MVBs. (**D**) Gold

particles on the outer (Ext, green) versus internal (Int, red) membrane of MVBs were quantified after 15 min at 37°C in cells expressing PAM-1/TS/AA or PAM-1/TS/DD.

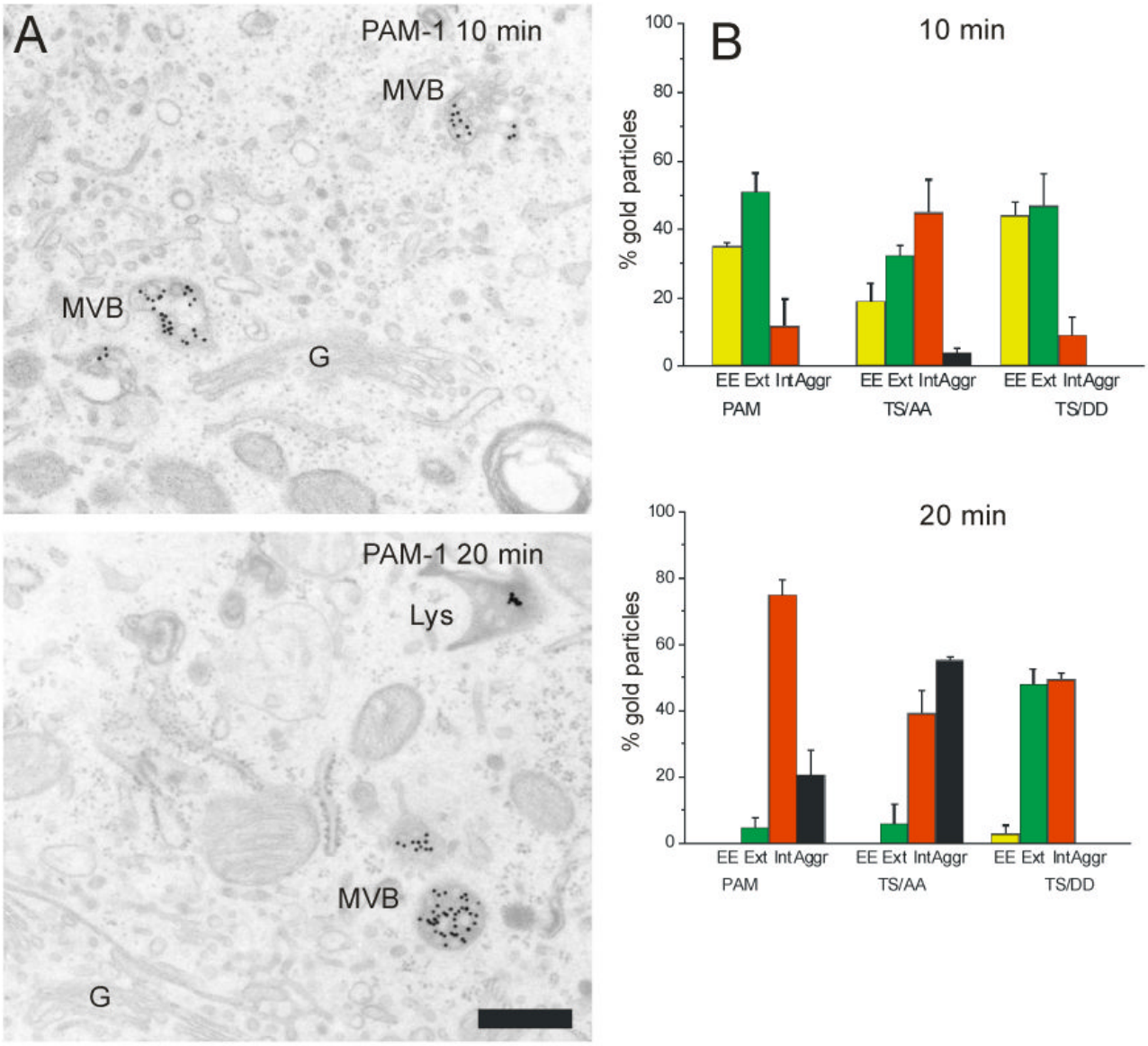


**Figure 8. Mutations affecting PAM cytosolic domain phosphorylation control entry into ILVs and lysosomes**

The three cell lines were labeled with PAM Ab/protein A-gold complexes on ice and allowed to internalize PAM Ab/protein A-gold complex for 10 or 20 min at 37°C. (**A**) Representative images are shown for PAM-1 cells; scale bar, 500 nm. (**B**) Quantification of gold particles in early endosomes (EE, yellow), outer (Ext, green) and internal (Int, red) membranes of MVBs and aggregated (Aggr, black) in MVBs or lysosomes (± SEM of two separate experiments).

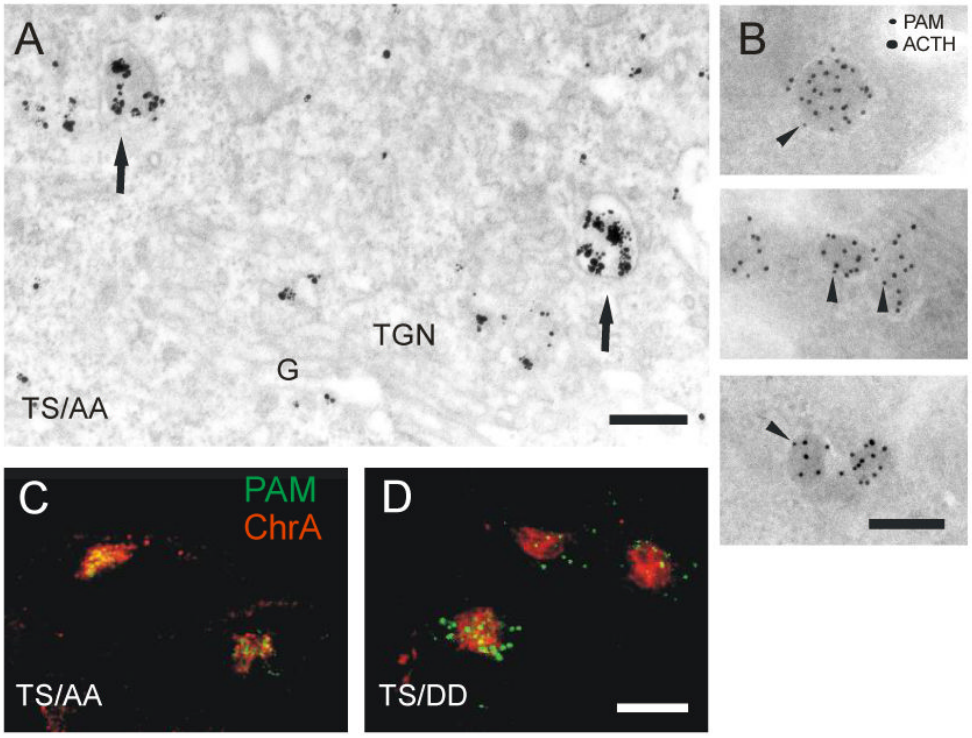


**Figure 9. Mutations affecting PAM cytosolic domain phosphorylation control return to SGs**

(**A**) Pre-embedding staining of PAM-1 antibody internalized for 20 min at 37°C by PAM-1/TS/AA cells. Label was seen in immature SGs (arrows). Scale bar, 200 nm. (**B**) PAM-1 antibody was internalized for 20 min at 37°C by PAM-1/TS/AA cells, the cells were fixed and prepared for cryosectioning. PAM-1 antibody in the sections was detected with 10 nm protein A-gold (arrowheads). After blocking, the sections were then stained with ACTH antibody detected with 15 nm protein A-gold. Scale bar, 200 nm. Antibody internalized for 20 min at 37°C by PAM-1/TS/AA (**C**) and PAM-1/TS/DD (**D**) cells was visualized along with with chromogranin A. Scale bar, 10 μm. The figures represent thin optical sections not including the tips of the cell processes.

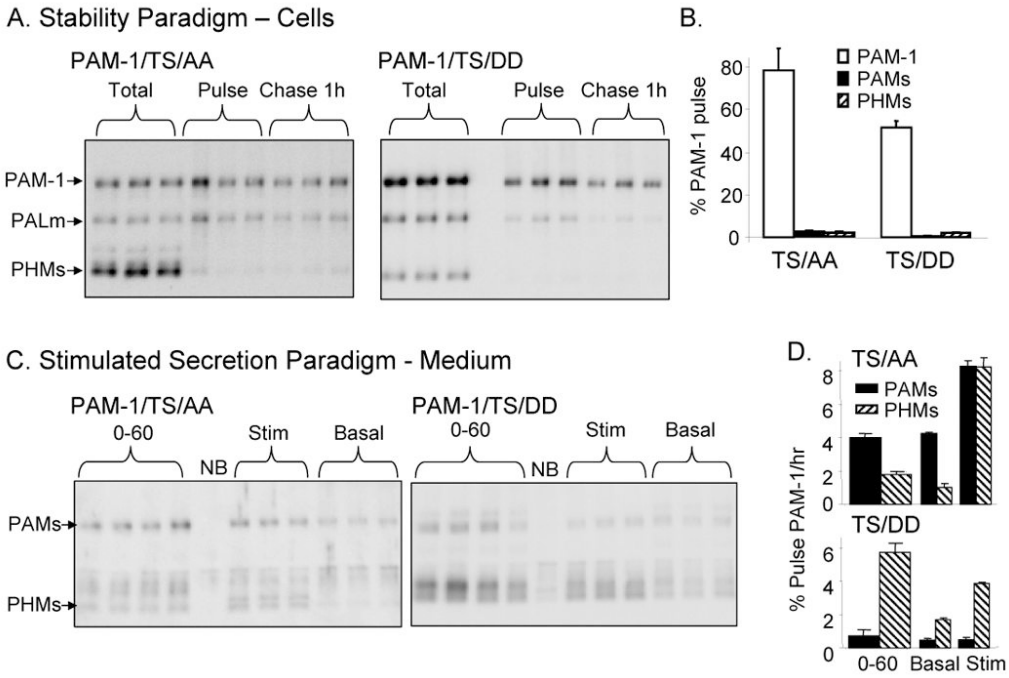


**Figure 10. Mutations affecting PAM cytosolic domain phosphorylation affect fate of surface biotinylated PAM-1**

(**A**) AtT-20 lines expressing PAM-1/TS/AA or TS/DD were analyzed using the biotinylation stability paradigm described in Fig. 2A; PAMs and PHMs secreted basally during the 1 h and 4 h chase periods were also quantified. (**B**) Data for the 1 h chase were quantified relative to biotinylated PAM-1. (**C**) The stimulated secretion biotinylation paradigm described in Fig. 1C was used to analyze PAM-1/TS/AA and TS/DD cells. (**D**) Secretion of biotinylated PAMs and PHMs during the 0-60 min chase and the subsequent 30 min Basal or Stimulated collection was quantified relative to intact, biotinylated PAM.